Check for updates

A study of the mechanical properties of the NEPE binders by molecular dynamic simulations and experiments

La Shi, [ID] Li Ren, Yang Li, Xiaolong Fu,* Saiqin Meng and Jiangning Wang

In this study, the crosslinking structures of nitrate ester plasticized polyether (NEPE) binders were constructed by a computational procedure. Based on the final crosslinking models, the glass transition temperatures, mechanical properties, and thermal expansion coefficients of polyethylene glycol400/multi-functional isocyanate (PEG400/N-100), polyethylene glycol400/toluene diisocyanate (PEG400/HDI), polyethylene glycol400/hexamethylene diisocyanate (PEG400/TDI) and polyethylene glycol400/isophorone diisocyanate (PEG400/IPDI) models were simulated by molecular dynamics, and could be confirmed by experiments. Then the bond-length distributions, conformation properties and cohesive energy densities were used to analyze in detail how the different cured structures influenced the mechanical and thermal properties. Furthermore, the radial distribution function, mean square radius of gyration, volume shrinkage and fraction free volume were calculated, which could directly explain the relationships between the intermolecular chains and macroscopical properties of the NEPE binders. Lastly, PEG400/N-100 and PEG400/HDI systems were chosen for the experiments. The dynamic mechanical analysis results explained that PEG400-HDI showed better flexibility and its T_g value was 45 °C lower than that of PEG400-N100. The mechanical properties illustrated that the ultimate tensile strength and Young's modulus of PEG400/N-100 were both to an extent higher than that of PEG400/HDI in the temperature range of −40 °C to 50 °C, according to the results provided by a universal tensile test machine. The experimental results were in good agreement with the simulation analysis. This work can help us to have an efficient comprehension on the crosslinking structures and micro-property relationships of the NEPE binders and act as a guidance for designing applicable polyurethanes in propellant applications.

1 Introduction

There has been a lot of effort put into the research performances of energetic polymer binders for solid rocket propellants.[1] Nitrate ester plasticized polyether (NEPE) propellants are new crosslinking solid propellants, which have a polyurethane network with excellent mechanical and thermal properties.[2,3] The function of the binder system is to form a three-dimensional (3D) space,[4,5] and stabilize plasticizers, oxidizing agents, additives and other propellant grains. The microstructure can affect the mechanical, viscoelastic and thermal properties, and the rocket motor could suffer a failure.[6,7] Therefore, it is essential to explore the correction between the microstructures and macro-properties.[8–11]

Molecular dynamics (MD) simulations of NEPE propellants have received increasing attention recently as a result of their capability to gain insightful structure–property information at the microscopic scale instead of experiments.[12–16] During the

Xi'an Modern Chemistry Research Institute, Xi'an 710065, China. E-mail: fuxiaolong204@163.com

curing stage, the hydroxyl groups of polyethylene glycol (PEG400) react with the isocyanate groups and produce polyurethane, and simulating the crosslinking of polymers is needed to modify the parameters repeatedly to gain useful insights. The crosslinking of polyurethanes can be affected by various factors, including the ratios of raw materials and conversion rates during the processing conditions.[17] To overcome these barriers, many scientists have attempted various methods, such as quantum mechanics, coarse grain molecular simulations, kinetic Monte Carlo methods and cutoff distance methods. When analyzing the crosslinked polymers generated by a mapping procedure, Komarov *et al.*[18] found that T_g increased with the increase in the degree of crosslinking. Schichtel *et al.*[19] explored a modified method to model the curing crosslink structure, minimizing high potential energy reaction groups with practical flexibility. Aniruddh *et al.*[10] replicated the polymerization process by a method called accelerated ReaxFF, which embraced the barrier energy, cutoff distance and the effect of molecular chemistry. Sun *et al.*[20] simulated polymers under two typical force fields. Hall *et al.*[21] created a new crosslink model construction technique, which

indicated the prediction of the glass transition temperature, which was in good agreement with experimental results. Shen et al.[22] discussed the effect of the crosslink density on the network topology by MD methods and experiments. Fankhänel et al.[23] used MD simulations with atomic strain to estimate the elastic interphase properties. Radue et al.[24] confirmed that MD simulations could be used to study the mechanical behavior of epoxies with the Reax force field. Yan et al.[25] controlled the cutoff distances gradually and made the final crosslink density to 90% by MD simulations. Okabe et al.[26] reproduced the actual curing reaction by MD methods and simulated the mechanical properties of epoxy resin, whose results confirmed the experimental data. Patil et al.[27] used numerical simulated methods to predict the thermomechanical changes of the curing compounds. Zhang et al.[28] simulated PEG at different polymerization degrees and found that E_{PEG} became more stable when the polymerization degree was 90%.

In this study, MD simulation techniques and experiments were applied for assessing the mechanical properties of the binder systems in the NEPE propellant. First, by controlling the reaction distance, different crosslinking degree structures were obtained. Then based on the equilibrium crosslink structure, whose crosslinking rate of OH group was 100%, the mechanical and thermodynamic properties were analyzed. Simultaneously, some more simulations, for example, bond-length distribution analysis, conformation properties, cohesive energy density, radial distribution function, mean square radius of gyration, volume shrinkage and fractional free volume were assessed to verify the associations between the crosslinking structure and mechanical and thermal properties in the four NEPE binder systems. Lastly, PEG400/N-100 and PEG400/HDI systems were chosen for the experiments, including the dynamic mechanical and uniaxial tensile analysis.

2 Models and methods

2.1 Molecular model construction details

The models were built by Materials Studio. The chemical structures of polyethylene glycol400 (PEG400), multi-functional isocyanate (N-100), toluene diisocyanate (TDI), hexamethylene diisocyanate (HDI) and isophorone diisocyanate (IPDI) are shown in Fig. 1. The PEG polymer chains were built with repeat units in the Builder Polymers module, and the mean molecular weight was 400 g mol^{-1}. All models were optimized with Compass II force field[29] in the Forcite module. The oxygen atoms of PEG400 were named as R2, and the carbon atoms of isocyanate in the curing agents (N-100, IPDI, HDI and TDI) were labeled as R1, which could be recognized by the procedure.

2.2 Computational details

2.2.1 The construction of blend systems and MD details. In this study, all the molecular dynamic simulations were performed in the Compass II force field to study the properties on the binders of NEPE propellants in the Materials Studio. The bends of PEG400/N-100, PEG400/HDI, PEG400/IPDI and PEG400/TDI were constructed in the Amorphous Cell module,
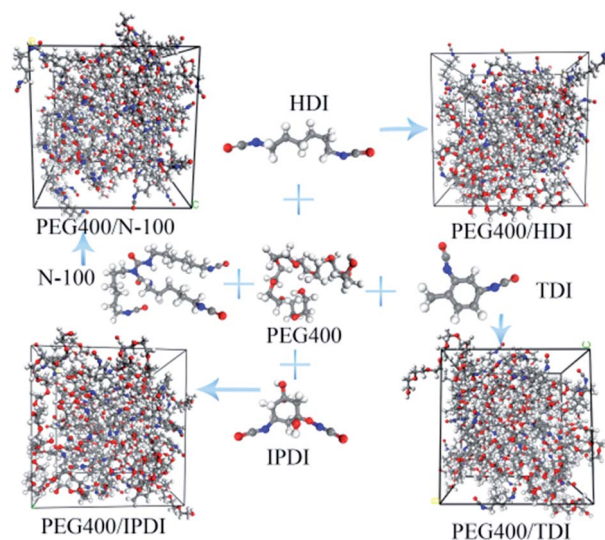

Fig. 1 Molecular structure of prepolymer (PEG), curing agents (N-100, IPDI, HDI, TDI) and the PEG400/N-100, PEG400/HDI,PEG400/TDI, PEG400/IPDI blends. Atoms: gray (C), white (H), red (O) and blue (N).

whose boxes were all 25.83 × 26.68 × 26.66 Å^3 at an initial density of 0.6 g cm^{-3}. The van der Waals and electrostatic interactions were set with the atom-based and Ewald methods, respectively. The original cutoff distance was set at 12.5 Å. From the 10 output frames, the one with the lowest energy was chosen. These structures were relaxed by 50 000 step energy minimization. Then, the amorphous bends needed annealing from 298 K to 598 K, with 20 K ramps per cycle and 5 annealing cycles. There were 200 ps NPT dynamics in every temperature ramp and 40 000 steps of the total number. Further, these bends were subsequently optimized for 400 ps with a time step of 1 fs, which involved selecting the NVT ensemble and NHL[30] thermostat at 298 K in the Forcite module, in which the decay constant was 1 ps. Then, the ensemble was converted into NPT, NHL thermostat and Berendsen[31] barostat under 10^{-4} GPa pressure and 5 000 000 energy deviation, with other parameters unchanged. When the temperature and energy were in equilibrium, the amorphous system reached a balance. Next, the cure reactions occurred between the isocyanates and hydroxide radicals of the equilibrium binder systems. The models of the NEPE binder system are shown in Fig. 1.

2.2.2 Curing simulation. Recently, MD simulation has been used to construct crosslinked structural models of polymers.[32,33] The crosslinking reaction between a prepolymer and curing agent containing isocyanate group follows the principle of addition polymerization. The curing reaction mechanism of the binders is presented in Fig. 2.
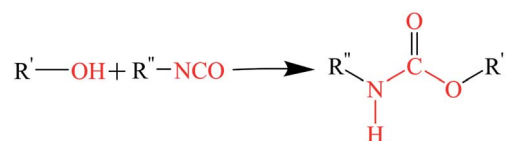

Fig. 2 Curing reaction mechanism.

The steps of the crosslinking mechanism algorithm are shown in Fig. 3, which were accomplished automatically by Perl scripts written according to the mechanism of the double bond addition reaction of alcohols with isocyanates. Some assumptions made are as follows: (i) the PEG400 chains and curing agents were selected equiprobably. Also, all the reactive groups, including the N=C=O and O–H, were assumed to be spheres of a certain radius. (ii) The reactive groups were activated when they met within a set distance. (iii) The activated groups shifted into the crosslinking groups. If there were no more reactive groups within the distance, the reaction radius was gradually added by 0.5 Å. The reaction would halt until the OH groups had run out. The conversion, temperature (T), min reaction radius (R_{min}), max reaction radius (R_{max}) and other parameters were stipulated. For example, the conversion (α) was 100%, T was 600 K and R_{min} and R_{max} were at 3.5 Å and 14 Å, respectively. When the active groups just met in the distance between R_{min} and R_{max}, the crosslinking reaction would happen and the atoms would be connected. If they were a cured group, there would be no reaction.

Finally, the crosslinked models were optimized, carried out by the molecular dynamic simulation in NVT and NPT ensembles. Furthermore, the optimized crosslinked models were annealed. All these parameters were identical to those in the section 2.1. The curing degree of binders is defined as the number of reacted hydroxyl sites over the total number hydroxyl sites of PEG400.

2.3 Materials and experiments

2.3.1 Materials. In this investigation, polyethylene glycol (PEG; CP) was provided by Sinopharm Chemical Reagent Co., Ltd and its average formula weight was 400 Dalton. Multifunctional isocyanate (N-100) with 5.32 mmol g^{-1} isocyanate group toluene diisocyanate (TDI; AR) was provided by Sinopharm Chemical Reagent Co., Ltd. Hexamethylene diisocyanate (HDI; 99% purity) was bought from Aladdin. Isophorone diisocyanate (IPDI; 99% purity) was provided by Shanghai Macklin Biochemical Co., Ltd. The chemical structures of main raw materials were shown Fig. 4. ALT-402 as the water remover was provided by Changde Ailite New Material Technology Co., Ltd. The NCO/OH molar ratio of prepolymer and curing agent was

1.5. After the two systems were cured and shaped in the oven, the binders were cut into standard sizes for the property tests.

2.3.2 Experiments. PEG400 needed drying with 2–3 wt% ALT-402 for 24 h. Then the prepolymer and curing agent blends of the binder were manually stirred homogeneously for 10 min and degassed for several minutes until no gas appeared in a vacuum oven at 70 °C. The mixed blends were then poured into the cuboid molds. Finally, the binder blends were put into a high temperature oven at 70 °C for 72 h until the crosslinking reaction was completed.

The dynamic mechanical properties of the samples were tested by dynamic mechanical analyzers (DMA850, Single Cantilever), fixed with a tensile clamp. The sample size prepared was 35 mm × 13 mm × 3 mm. The test temperature was swept from −120 °C to 100 °C with the liquid nitrogen refrigerant. The heating rate was 3 °C min^{-1} and the loading frequency was 1 Hz. The mechanical properties were obtained at a crosshead speed of 500 mm min^{-1} by a universal testing machine (AG-X plus, 5 kN, Shimadzu, Japan) by processing into JANNAF dog bones (length 75 mm × narrow parallel width 4 mm × thickness 2 mm) as shown in Fig. 5.

3 Results and discussion

3.1 Simulation parts

3.1.1 Glass transition temperature. For amorphous polymers, a conversion could happen from a malleable liquid or rubbery state to a glassy state at the glass transition temperature (T_g).[34–37] Therefore, T_g is a critical thermal property parameter of polyurethane, which provides an effective temperature range in
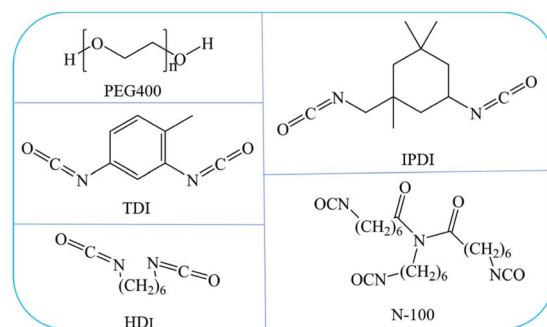

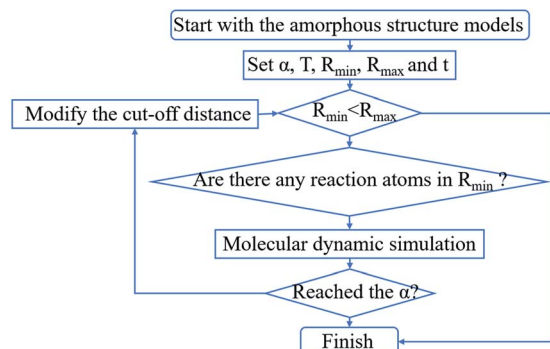Fig. 4 Molecular formulas of PEG400, TDI, IPDI, N-100 and HDI.

Fig. 5 (a) and (b) Cured samples of PEG400/N-100 and PEG400/HDI systems.

Fig. 3 Flow chart of the crosslinking reaction algorithm.

applications. If cooled under T_g, the pliability and flexibility of binders would disappear. The hardness and brittleness would appear concurrently. Therefore, the mechanical and thermal properties could be abundantly changed around T_g. The mean square displacement, specific volume and specific density could be used to estimate the value of T_g by changing the molecular mobility of polymer chains at different temperatures.[8] T_g can also be obtained by the intersection of two linear lines that are fitted to the specific density *vs.* temperature data at the low and high temperature range. The system was simulated *via* cooling from 598 K to 208 K at a cooling rate of 20 K per 50 ps in the NPT ensemble and the specific density value was obtained as the average of five cycles. According to the MD simulation and influence of the polymer density and diffusion on some properties, Shen[22] indicated that the structures of crosslinks could slow down the long chain dynamics and lead to a higher glass transition temperature. As seen in Fig. 6, the T_g values of PEG400/N-100, PEG400/HDI, PEG400/TDI and PEG400/IPDI are 335 K, 304 K, 283 K and 292 K, respectively. The T_g simulated value accuracy was influenced by the computation progress.

3.1.2 Mechanical properties. The mechanical properties of the NEPE propellant is mainly affected by the prepolymer, curing agent and crosslinking products. The static constant strain method was used to calculate the mechanical properties of the system. That is, a small strain was applied to the system to make the model deform in the *xy*, *xz* and *yz* planes. Through the response of the system, the stiffness matrix could be obtained. For the elastic mechanics, the relationship between stress and strain could be described by the generalized Hooke's law as eqn (1).

$$\sigma_{ij} = C_{ij}\varepsilon_{ij} \qquad (1)$$

where the σ_{ij} are the stress vectors and ε_{ij} $(i, j = 1, 2, 3)$ are the strain vectors. C_{ij} is the elastic constant and could be calculated by the $[C_{ij}]$ stiffness matrix.
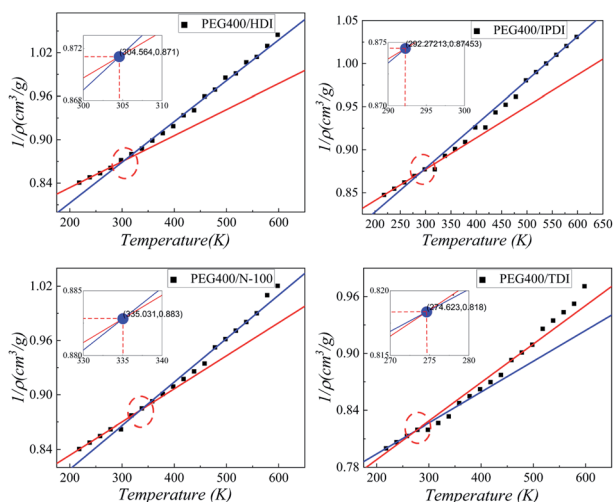

Fig. 6 The glass transition temperatures of PEG400/IPDI, PEG400/HDI, PEG400/N-100 and PEG400/TDI binder systems.

In the molecular simulation, stress could be provided from eqn (2).

$$\sigma_{ij}^{\alpha} = -\frac{1}{V^{\alpha}} \sum_{\alpha} \left(m^{\alpha} u_i^{\alpha} u_j^{\alpha} + \sum_{\beta} r_i^{\alpha\beta} f_j^{\alpha\beta} \right) \qquad (2)$$

where m^{α}, u_i^{α}, u_j^{α} are the mass and *i*th and *j*th velocity of the α atom; V^{α} is the volume of the system; $r_i^{\alpha\beta}$ and $f_j^{\alpha\beta}$ are the *i*th distance and *j*th force between α and β atoms.

For the isotropic polymers, the stiffness matrix could provide the effective Lame's constants λ and μ according to the equations below.

$$\lambda = \frac{1}{6}(C_{12} + C_{13} + C_{21} + C_{23} + C_{31} + C_{32}) \qquad (3)$$

$$\mu = \frac{1}{3}(C_{44} + C_{55} + C_{66}) \qquad (4)$$

Lastly, the Young's modulus E, shear modulus G, bulk modulus K and Poisson' ratio ν could be calculated from the following equations.

$$E = \frac{\mu(3\lambda + 2\mu)}{\lambda + \mu} \qquad (5)$$

$$G = \mu \qquad (6)$$

$$K = \lambda + \frac{2}{3}\mu \qquad (7)$$

$$\nu = \frac{\frac{1}{2}\lambda}{\lambda + \mu} \qquad (8)$$

The mechanical properties of the NEPE binders at 273.15 K were calculated and are listed in Table 1, obtained through formulations eqn (3)–(9) by MD simulations. As the results show, PEG400/HDI has the highest Young's modulus 8.272 GPa and shear modulus 3.087 GPa but PEG400/IPDI has the highest bulk modulus 7.730 GPa. This indicates that the curing agents have an important impact on the mechanical properties.

3.1.3 Thermal expansion coefficient. The coefficient of thermal expansion (CTE) is the regular coefficient for the geometric properties changing with temperature under the effect of thermal expansion and cold contraction. The mean volume coefficient of thermal expansion β is defined as below:

$$\beta = \frac{1}{3V}\left(\frac{dV}{dT}\right)_P \qquad (9)$$

where V, P and T represent the original volume, constant pressure and temperature, respectively.

CTE would fluctuate dramatically around T_g, thus the volume of the high and low temperature range is chosen to obtain β. The values of CTE were calculated from the volume as a function of temperature, referred to in eqn (9). The results of the volume coefficient of thermal expansion are listed in Table 2. For the four binder systems, CTE below T_g were appreciably smaller than the values above T_g. CTE from the glassy state to

Table 1 Mechanical properties of the NEPE binders at 273.15 K

System	Bulk modulus (GPa)	Shear modulus (GPa)	Young's modulus (GPa)	Poisson ratio
PEG400/N-100	8.644	2.298	6.332	0.378
PEG400/HDI	8.617	3.087	8.272	0.340
PEG400/TDI	8.546	2.254	6.215	0.379
PEG400/IPDI	7.730	2.532	6.849	0.352

Table 2 CET values of the NEPE binders

System	Below T_g (K^{-1})	Above T_g (K^{-1})
PEG400/N-100	4.32×10^{-4}	5.50×10^{-4}
PEG400/HDI	1.24×10^{-4}	2.80×10^{-4}
PEG400/TDI	6.12×10^{-5}	3.03×10^{-4}
PEG400/IPDI	1.54×10^{-4}	2.61×10^{-4}

rubbery state changed most significantly in the PEG400/TDI system.

3.1.4 Bond-length distribution analysis. In order to analyze the crosslinking structure, the bond-length distributions of the curing agent (N-100), prepolymer (PEG400) and final cross-linking structure were calculated. Fig. 7 shows the bond-length distribution of the binders (a) N-100, PEG400 and PEG400/N-100, (b) HDI, PEG400 and PEG400/HDI, (c) TDI, PEG400 and PEG400/TDI and (d) IPDI, PEG400 and PEG400/IPDI, respectively. From the comparison analysis, the bond-length distributions of the C–H, C–O and C–C bonds of PEG400 were almost the same as the curing agents (N-100, HDI, TDI and IPDI). The final crosslinking structures presented some new bonds, which proved that the curing reaction occurred between the prepolymer and curing agent. The length of C–H, C=O, N=C and C–N bonds of the crosslink structure changed at the left of the original monomers in all the systems. Also, from the molecular
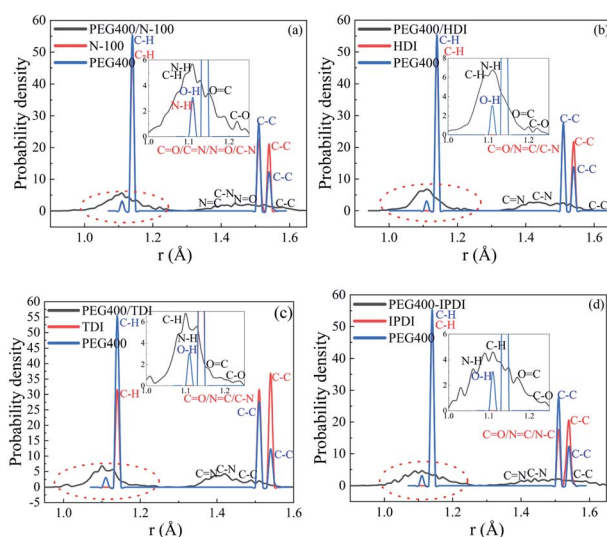
model in Fig. 7, the bond details are provided between the no curing monomers and cured structures.

3.1.5 Conformation properties. It is well known that there is a close connection between the thermomechanical properties of polyurethane and flexibility of the molecular chain segments. The more flexible the molecular chains are, the lower the values of T_g and moduli are. Under a specific torsion, the synergetic rotational energy barrier could be reversed. Also, the flexibility of the molecular chains would trail off with the higher synergetic rotational energy barrier. After the curing reaction, PEG400 and curing agents shifted into longer molecular chains, and we could calculate the synergetic rotational energy barrier related to some specific bonds to realize flexibility.[38] Herein, the new C–O bond of the crosslinking structure and other pointed bonds could be chosen at the same time. Then the energies associated with the two particular bonds could be worked out. Fig. 8 shows the torsion rotation of the special bonds $\varphi 1$ and $\varphi 2$ in the NEPE binders, PEG400/N-100, PEG400/HDI, PEG400/TDI and PEG400/IPDI. Moreover, the total energy of the special bonds $\varphi 1$ and $\varphi 2$ are shown in Fig. 9. PEG400/HDI has the lowest synergetic rotational energy barrier of 473.566 kcal mol^{-1}, while PEG400/IPDI has the highest at 1159.808 kcal mol^{-1}, and PEG400/N-100 and PEG400/TDI have the values 766.194 kcal mol^{-1} and 990.0489 kcal mol^{-1}, respectively. Therefore, PEG400/HDI has better stability than PEG400/N-100. This result revealed a similar tend with simulated T_g and mechanical properties.

3.1.6 Cohesive energy density. The cohesive energy density (CED) is closely correlated to intermolecular connections, which usually provide a perception of how the interchain relations
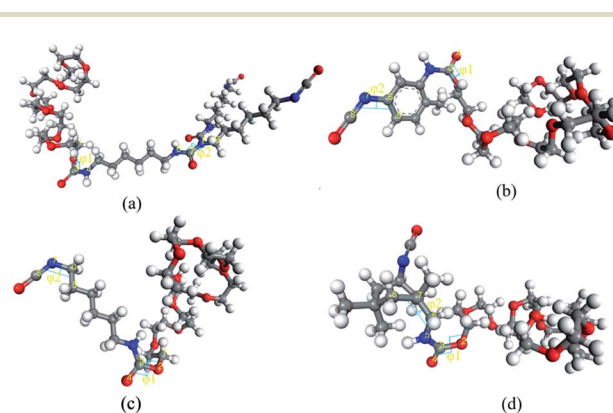

Fig. 7 The bond-length distribution of the NEPE binders: (a) PEG400/N-100, (b) PEG400/HDI, (c) PEG400/TDI and (d) PEG400/IPDI.

Fig. 8 The torsion rotation of the special bonds $\varphi 1$ and $\varphi 2$ in the NEPE binders: (a) PEG400/N-100, (b) PEG400/HDI, (c) PEG400/TDI, (d) PEG400/IPDI.
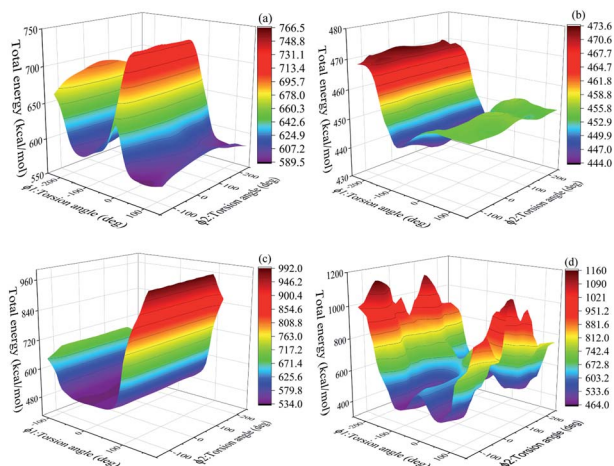
Fig. 9 Total energy of the special bonds $\varphi 1$ and $\varphi 2$ in the NEPE binders. (a) PEG400/N-100, (b) PEG400/HDI, (c) PEG400/TDI and (d) PEG400/IPDI.

influence the thermal and mechanical properties, especially T_g and theoretical moduli in the crosslinking structure of polyurethane.[11,39,40]

The cohesive energy (E_{coh}) is described as the average energy required per mole of the system if all intermolecular forces were overcome. It can be calculated by the following eqn (10).[41]

$$E_{coh} = \langle E_{inter} \rangle = \langle E_{total} \rangle - \langle E_{intra} \rangle \tag{10}$$

where E_{total} is the total energy of the system, E_{inter} is the total energy among all molecules and E_{intra} is the intramolecular energy.

CED is the cohesive energy density per unit volume, and is given by the formula (11) below.

$$CED = \frac{E_{coh}}{V} \tag{11}$$

where E_{coh} is the internal energy, V is the volume and CED is the cohesive energy density, which is the ratio of E_{coh} to V.

The simulated cohesive energy density results for the NEPE binders in the four systems are presented in Table 3. Here, PEG400-N100 has the highest value 8.590×10^8 J m^{-3}, which shows that the intermolecular forces in PEG400-N100 are the strongest. On the contrary, PEG-IPDI with 2.402×10^8 J m^{-3} has the weakest intermolecular forces among the different binder systems in this study. Through the CED analysis, the T_g and modulus of PEG400-N100 were found to be the highest, and are highly consistent with the properties determined by molecular dynamic simulations.

3.1.7 Radial distribution function. The radial distribution function (RDF) could be utilized for the evaluation of specific

atoms in the curing process, reflecting the shape of the cured networks and studying the order, type of interactions and the mechanical property mechanism of the NEPE binders. When an atom is close to other atoms, RDF describes how the atoms stack up and how close their bonds are to each other. In general, RDF shows a long-range peak for crystals because of their ordered structure, and only a short-range peak for the amorphous materials. RDF describes the probability of finding an A atom around a radius r of the special B atom, and it can be determined from eqn (12).

$$g_{AB}(r) = \frac{n_{AB}(r)}{4\pi r^2 dr \left(\dfrac{N_A N_B}{V} \right)} \tag{12}$$

where N_A and N_B are the number of A atoms and B atoms, respectively, V is the volume of blends and $n_{AB}(r)$ is the total number of AB groups within the distance from $\left(r - \dfrac{1}{2} dr \right)$ to $\left(r + \dfrac{1}{2} dr \right)$.

In brief, the intermolecular interactions usually refer to the hydrogen bonding (2.0 Å $\leq r <$ 3.1 Å), van der Waals forces 3.1 Å $\leq r <$ 5 Å and weak van der Waals forces 5 Å $< r$.[42,43] Fig. 10 shows the peak position (r) and $g(r)$ intensities of the four kinds of NEPE binder systems. For the radial distribution functions of the NEPE binders, there are some peaks from the distance 1.1 Å to 2.0 Å, corresponding to the bond-length distribution. Comparing and contrasting intramolecular chemical bonding and intermolecular nonbonding, the hydrogen bonding and van der Waals forces are smaller forces.

Most of the imines of various groups in polyurethane can form hydrogen bonds, with most of them formed with a carbonyl group in the hard segment, and a small part formed between ether the oxygen group or ester carbonyl group in the soft segment.[44,45] Fig. 11 shows the radial distribution functions between the donor H atoms and accepter 0 atoms or N atoms. The first peak of the four systems were all around 1.1 Å between H and N atoms, which were the intramolecular N–H bonds of the crosslinking structure. The most obvious peaks were in the distance range from 2 Å to 3.1 Å, which meant that strong
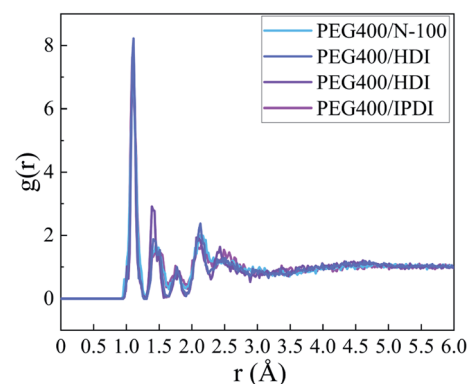
Table 3 Cohesive energy density of the NEPE binders

System	PEG400-N100	PEG400-HDI	PEG400-TDI	PEG400-IPDI
CED (J m^{-3})	8.590×10^8	4.449×10^8	4.527×10^8	2.402×10^8

Fig. 10 Radial distribution function of the NEPE binders in PEG400/N-100, PEG400/HDI, PEG400/TDI and PEG400/IPDI systems.
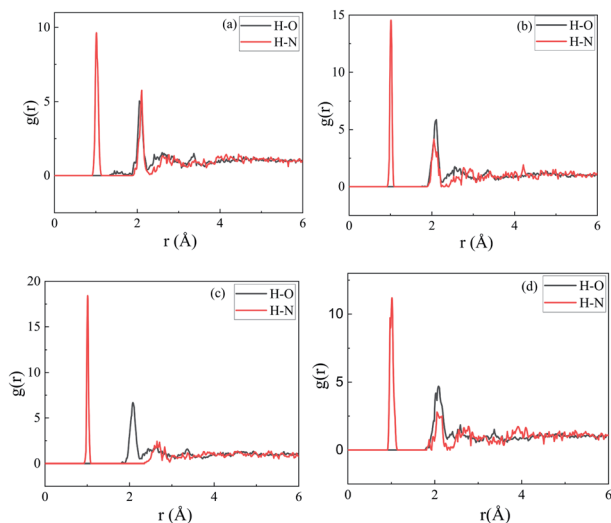
Fig. 11 Radial distribution function among H−O and H−N atoms: (a) PEG400/N-100, (b) PEG400/HDI, (c) PEG400/TDI and (d) PEG400/IPDI.

hydrogen bonding existed in the crosslinking structure. Also, the hydrogen bonding of PEG400-TDI was partly weaker than in others. These analysis results are consistent with the wonderful mechanical properties of the NEPE binders from the simulations. Further, vdW and hydrogen bonding played important roles in the crosslinking structure of this study.

3.1.8 Mean square radius of gyration. The mean square radius of gyration (MSRG) could explain the polymer cluster size, while the flexibility and temperature resistance of the binders could be explained by analyzing the macroscopical properties of the polymer. The calculation formula for MSRG is defined in eqn (13). The distribution curves of the PEG/N-100 cured polymer's radius of gyration in blended nitrate plasticizer and the curves of the PEG/N-100 cured polymer's radius of gyration with time are shown in Fig. 12.

$$R_g{}^2 = \frac{\sum m_i r_i{}^2}{\sum m_i} \tag{13}$$

If the polymer chain contains many chain units, and the mass of each chain unit is m_i, then the distance from the center of mass of the polymer chain to the first chain unit is r_i.
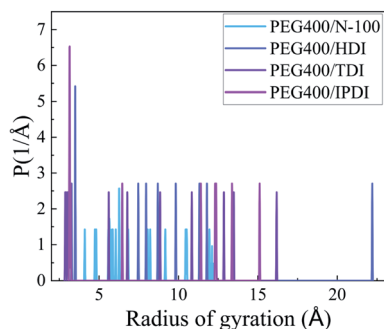

Fig. 12 Distribution of MSRG of the NEPE binders in four systems.

The mean square radius of gyration curves of the NEPE binders about different systems shown in Fig. 12. The radius of gyration of PEG400-N100, PEG400-HDI, PEG400-TDI and PEG400-IPDI widely ranged from 4.06 Å to 12.27 Å, 3.36 Å to 22.24 Å, 2.83 Å to 16.24 Å and 3.09 Å to 15.15 Å, respectively. The least dispersed radius of gyration distribution and lowest peak were for PEG400-N100, while PEG400-HDI had the most scattered one, which reflected that the latter had a small polymer chain nematic size. This analysis is in accordance with the earlier T_g and conformation properties.

3.1.9 Volume shrinkage and fraction free volume. During the crosslink reaction progress, the volume of the blends expand or shrink because of the interconnection changes among molecular chains. Usually, the higher the degree of crosslink is, the more the volume would shrink. Comparing the optimized original blends, the volume shrinkages of crosslinked PEG400/N-100, PEG400/HDI, PEG400/TDI and PEG400/IPDI were 1.14%, 4.48%, 5.17% and 2.17%, respectively. Obviously, the different curing agents had an important influence on the volume variation.

The mechanical and thermal properties of polyurethane are largely determined by the free volume and movement of molecular chain segments. According to the free volume theory, the volume V_T of liquid and solid substances consists of two parts, one is the van der Waals volume occupied by molecules, V_0, and the other is the unoccupied volume, V_f, namely the free volume. Due to the different volumes of different polymer systems, it is generally not possible to directly compare the free volume of each system. The distributions of V_0 and V_f are shown in Fig. 13, and the calculated results are shown in Table 4. Therefore, the fractional free volume (FFV) was introduced to represent the relative size of the free volume, and is expressed by eqn (14).

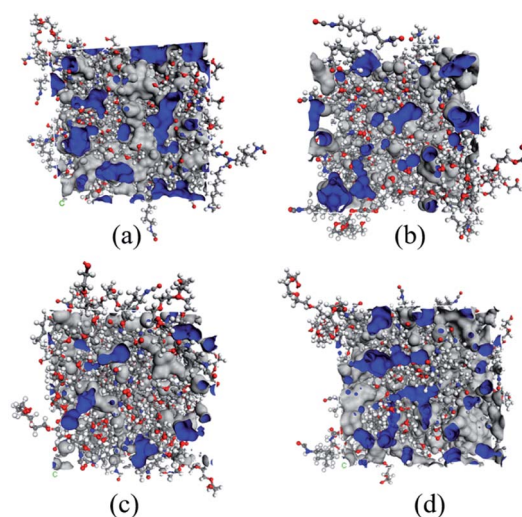$$\text{FFV} = \frac{V_f}{V_0 + V_f} \times 100\% \tag{14}$$

Fig. 13 The free volume distribution of the NEPE binders: (a) PEG400/N-100, (b) PEG400/HDI, (c) PEG400/TDI and (d) PEG400/IPDI.

Table 4 The results of V_0, V_f and FFV in four NEPE binder systems

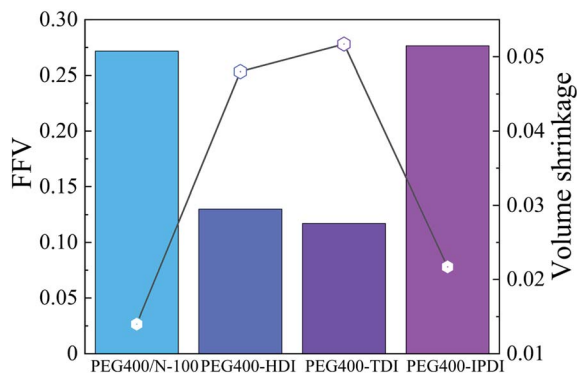| System	V_0 (Å³)	V_f (Å³)	FFV (%)
PEG400/N-100	22283.14	8312.28	27.17
PEG400/HDI	17135.73	2560.54	13.0
PEG400/TDI	16409.96	2176.41	11.71
PEG400/IPDI	18516.52	7071.24	27.64

Fig. 14 Volume shrinkage and fractional free volume of NEPE binders.

Also, the free volume fraction and volume shrinkage of NEPE binder in the four systems are presented in Fig. 14. The FFV values of PEG400/N-100, PEG400/HDI, PEG400/TDI and PEG400/IPDI were 27.17%, 13.0%, 11.7% and 27.64%, respectively. This indicates that the spatial crosslinking structure of PEG400/N-100 and PEG400/IPDI can supply more interspace. In addition, these also resulted in volume shrinkage during the curing progress.

3.2 Experimental parts

3.2.1 Dynamic mechanical analysis. The viscoelastic behavior of the NEPE binders could be analyzed with a dynamic condition by a dynamic mechanical analyzer (DMA). Fig. 15 shows the storage modulus E', loss modulus E'' and loss factor (tan δ) of two different binder systems as a function of temperature at the frequency 1 Hz. On account of the interactions being weakened among the molecular chains, the E' of the two systems were in a continuous downward trend with increasing temperature. The storage modulus of PEG-HDI was higher than that of PEG-N100 at the same temperature and was influenced more significantly by the temperature change. The loss modulus is a mechanical loss, which describes the phenomenon of energy transformation into heat when materials are in viscosity deformation. Although the loss modulus of PEG400/N-100 was higher than that of PEG-HDI below −50 °C, PEG400/HDI quickly went beyond the latter. When the temperature increased, the ability of the polymer chains to move and deform viscously would be aggrandized.

Tan δ is equal to the ratio of the loss modulus to the storage modulus and its curve peak point corresponding temperature is defined as T_g.[46] The loss factor tan δ curves of the various samples are shown in Fig. 16. It is obvious that the T_g values of
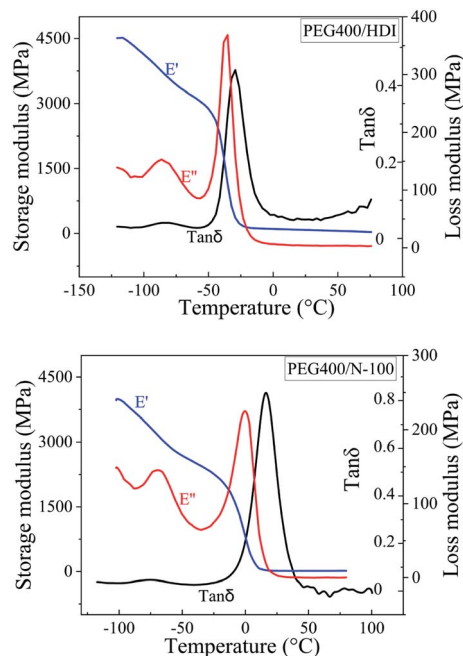

Fig. 15 The DMA curves of the NEPE binders at 1 Hz.

PEG400/N-100 and PEG400/HDI are 15.74 °C and −29.29 °C, respectively. PEG400/HDI showed better flexibility and the value of T_g was 45 °C lower than that of PEG400/N-100. The simulation T_g values were somewhat higher than the DMA experiment results, mainly because the cooling rates of the simulated temperature differed a lot from the real experimental sets.[47]

3.2.2 Mechanical properties of the NEPE binders. The mechanical properties of the NEPE binder PEG400/N-100 and PEG400/HDI systems, including the ultimate tensile strength (σ_m), strain at break (ε_b), Young's modulus (E_{exp}) and the standard deviations, performed under a wide temperature range from −40 °C to 50 °C are presented in Table 5. The continuous stress–strain curves of the two NEPE binder systems are exhibited in Fig. 17. Five samples were tested for each binder system, and the final results are presented in Table 5 as a reference to GB_T528_2005.
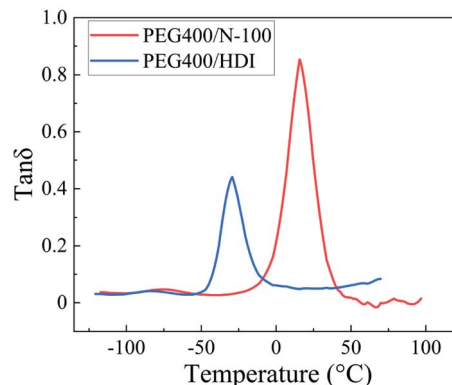

Fig. 16 The loss factor curves of the NEPE binder.

Table 5 Mechanical properties of the NEPE binders at −40 °C, 20 °C and 50 °C

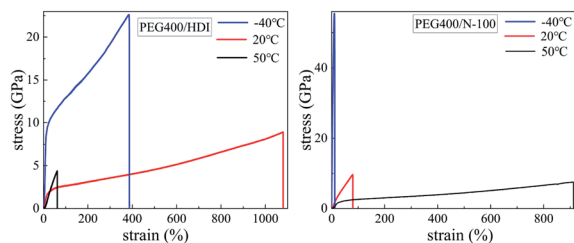| System	T (°C)	σ_m (MPa)	ε_b (%)	E_{exp} (MPa)
PEG400/N-100	−40	55.45 ± 10.45	10.18 ± 1.38	5752 ± 363.32
	20	9.63 ± 0.02	81.70 ± 2.45	98 ± 35.50
	50	8.98 ± 1.65	862.98 ± 40.68	63 ± 10.20
PEG400-HDI	−40	13.63 ± 1.65	255.62 ± 78.02	1558 ± 220.45
	20	6.74 ± 1.58	1277.26 ± 144.82	74 ± 11.00
	50	4.38 ± 0.91	61.48 ± 8.85	40 ± 6.53

Fig. 17 The stress−strain curves of NEPE binder systems.

In the initial loading stage, the steep rise trends indicated the high elastic modulus of the NEPE binders. The two binder systems showed similar behaviors at different testing temperatures. The stress–strain curves reached a maximum tensile strength and then the curve curl stopped, corresponding to the break strain.

Obviously, the σ_m and E_{exp} of both systems decreased gradually with the increase in temperature. These phenomena mainly resulted from the freezing movements of the molecular chains and more external force would be needed at a lower temperature. When the temperature was −40 °C, *i.e.* under the glass transition temperature, the σ_m and E_{exp} of PEG400/N-100 and PEG400/HDI showed ideal values of 55.45 ± 22.45 MPa and 13.63 ± 1.65 MPa, 5752 ± 363.32 MPa and 1558 ± 220.45 MPa, respectively. These results confirmed the DMA analysis that the mechanical properties would change a lot around the glass transition temperature. Furthermore, the σ_m and E_{exp} of PEG400/N-100 were consistently higher than the values of PEG400/HDI at the same temperature and the former had a tougher binder system. The reason was that the curing agent N-100 modified by HDI would present a more perfect 3D network in the NEPE binder system. The elongation at break of PEG400/N-100 was reduced when the temperature increased, while the ε_b values of PEG400/HDI would increase first and decrease later with the rising temperature. Generally speaking, the uniaxial tensile analytical results were in good agreement with the DMA results.

4   Conclusions

In this paper, the molecular dynamics simulation combined with experimental ways were applied to study how the crosslinking molecular structure was connected with the mechanical and thermal properties of the NEPE binders in four different polyurethane systems, namely PEG400/N-100, PEG400/HDI, PEG400/TDI and PEG400/IPDI. Further, the following results are presented.

To begin with, we constructed the basic blend model, obtained the high crosslinking (100%) structure by Perl scripts and optimized this until the system reached equilibrium.

Then, the glass transition temperature of PEG400/N-100, PEG400/HDI, PEG400/TDI and PEG400/IPDI were found to be 335 K, 304 K, 283 K and 292 K, respectively. The simulation results for the mechanical properties indicated that PEG400/HDI had the highest bulk modulus, shear modulus and Young's modulus among the four systems at 273.15 K. As expected, the thermal expansion coefficient shifted from below T_g to above T_g. The bond-length distributions of the original prepolymer and curing agents all differed from the final crosslink structure, including the appearance of some new bonds (C–O) and some old bond positions changed. The conformation properties analysis proved that PEG400/HDI had the lowest synergetic rotational energy barrier and PEG400/IPDI had the highest one. The cohesive energy density results verified that PEG400-N100 had the highest value of 8.590×10^8 J m^{-3} and PEG-IPDI had the least value of 2.402×10^8 J m^{-3}. Strong hydrogen bonding was found in the crosslink structure through the radial distribution function. PEG400-N100 exhibited the most regular radius of gyration distribution, but PEG400-HDI built the most dispersive one. The volume shrinkage and fractional free volume results verified that the mechanical properties were closely connected with the 3D network.

Lastly, the dynamic mechanical analysis results indicated that PEG400-HDI showed better flexibility and the value of T_g was 45 °C lower than that of PEG400-N100. The mechanical property data demonstrated the better flexibility of the PEG400/HDI system connected with the significant broad elongation at break. The maximal tensile stress and Young's modulus corresponded to the crosslink structure analysis by the simulation methods.

Conflicts of interest

There are no conflicts of interest to declare.

Acknowledgements

References

1 Y. Wang, H. Rong, X. Zhang, Y. Chen, W. Luo, Y. Liu, W. Yao and Y. Tian, *Propellants, Explos., Pyrotech.*, 2021, **46**, 950–961.

2 C. M. Roland and B. P. Mason, *Rubber Chem. Technol.*, 2019, **92**, 1–24.

3 H. Tan, *The Chemistry and Technology of Solid Rocket Propellant*, Beijing Institute of Technology Press, 2015.

4 R. G. Stacer and D. M. Husband, *Propellants Explos. Pyrotech.*, 1991, **16**, 167–176.

5 W. Xu, J. Deng and l. Zhang, *J. Solid Rocket Technol.*, 2010, **33**, 560–563.

6 Y. Chen, Y. Liu and H. Tan, *Chin. J. Explos. Propellants*, 2008, **31**, 56.

7 W. e. Wu, C. Chen, X. Fu, C. Ding and G. Wang, *Propellants, Explos., Pyrotech.*, 2017, **42**, 541–546.

8 X. Yang, Y. Wan, X. Wang, Y. Fu, Z. Huang and Q. Xie, *Composites, Part B*, 2019, **164**, 659–666.

9 Z. Yu, W. Wang, W. Yao, W. Zhang, W. Xie, Y. Liu, Y. Zhao, H. Tan and Y. Chen, *J. Energ. Mater.*, 2021, **39**, 74–84.

10 A. Vashisth, C. Ashraf, C. E. Bakis and A. V. Duin, *Polymer*, 2018, **158**, 354–363.

11 W. Zhang, Q. Yang, W. Zhong, S. Gang and X. Yang, *React. Funct. Polym.*, 2017, **111**, 60–67.

12 X. Fernàndez-Francos, À. Serra and X. Ramis, *Eur. Polym. J.*, 2014, **53**, 22–36.

13 G. Wang, S. Hou, W. Wu and H. Li, *J. Solid Rocket Technol.*, 2015, **38**, 684–688.

14 M. An, B. Demir, X. Wan, H. Meng, N. Yang and T. R. Walsh, *Adv. Theory Simul.*, 2019, **2**, 1800153.

15 P. Zhang, T. Li, S. Liu and J. Deng, *Comput. Mater. Sci.*, 2020, **171**, 109135.

16 L. A. Richards, A. Nash, M. Phipps and N. Leeuw, *New J. Chem.*, 2018, **42**, 17420–17428.

17 K. Chen, S. Yuan, X. Wen, C. Sang and Y. Luo, *Propellants, Explos., Pyrotech.*, 2021, **46**, 428–439.

18 P. V. Komarov, C. Yu-Tsung, C. Shih-Ming, P. G. Khalatur and P. Reineker, *Macromolecules*, 2007, **40**, 8104–8113.

19 J. J. Schichtel and A. Chattopadhyay, *Comput. Mater. Sci.*, 2020, **174**, 109469.

20 Y. Sun, C. Lin, C. Liu, Y. Zhang and X. Du, *Comput. Mater. Sci.*, 2018, **143**, 240–247.

21 S. A. Hall, B. J. Howlin, I. Hamerton, A. Baidak, C. Billaud and S. Ward, *PLoS One*, 2012, **7**, e42928.

22 J. Shen, X. Lin, J. Liu and X. Li, *Macromolecules*, 2019, **52**, 121–134.

23 J. Fankhänel, B. Arash and R. Rolfes, *Composites, Part B*, 2019, **176**, 107211.

24 M. S. Radue, B. D. Jensen, S. Gowtham, D. R. Klimek-Mcdonald, J. A. King and G. M. Odegard, *J. Polym. Sci., Part B: Polym. Phys.*, 2018, **56**, 255–264.

25 S. Yan, W. Verestek, H. Zeizinger and S. Schmauder, *Polymers*, 2021, **13**, 3085.

26 T. Okabe, Y. Oya, K. Tanabe, G. Kikugawa and K. Yoshioka, *Eur. Polym. J.*, 2016, 78–88.

27 A. S. Patil, R. Moheimani and H. Dalir, *Therm. Sci. Eng. Prog.*, 2019, **14**, 100419.

28 P. Zhang, A. Pang, G. Tang and J. Deng, *Appl. Surf. Sci.*, 2019, **493**, 131–138.

29 H. Sun, Z. Jin, C. Yang, R. L. C. Akkermans, S. H. Robertson, N. A. Spenley, S. Miller and S. M. Todd, *J. Mol. Model.*, 2016, **22**, 47.

30 B. Leimkuhler, E. Noorizadeh and O. Penrose, *J. Stat. Phys.*, 2011, **143**, 921–942.

31 H. J. Berendsen, J. V. Postma, W. F. Van Gunsteren, A. DiNola and J. R. Haak, *J. Chem. Phys.*, 1984, **81**, 3684–3690.

32 P. Zhang, J. Yuan, A. Pang, G. Tang and J. Deng, *Composites, Part B*, 2020, **195**, 108087.

33 J. Konrad, R. H. Meißner, E. Bitzek and D. Zahn, *ACS Polym. Au*, 2021, **1**, 165–174.

34 J. Pascault and R. Williams, *J. Polym. Sci., Part B: Polym. Phys.*, 1990, **28**, 85–95.

35 N. R. Jadhav, V. L. Gaikwad, K. J. Nair and H. M. Kadam, *Asian J. Pharm.*, 2009, **3**, 82–89.

36 G. Roudaut, D. Simatos, D. Champion, E. Contreras-Lopez and M. Le Meste, *Innovative Food Sci. Emerging Technol.*, 2004, **5**, 127–134.

37 J. Forrest, K. Dalnoki-Veress, J. Stevens and J. Dutcher, *Phys. Rev. Lett.*, 1996, **77**, 2002.

38 K. Fu, Q. Xie, L. Fangcheng, Q. Duan and Z. Huang, *Polymers*, 2019, **11**, 975.

39 Y. Qing, X. Li, L. Shi, X. Yang and G. Sui, *Polymer*, 2013, **54**, 6447–6454.

40 G. Liang, Q. Zhang, H. Li, S. Yu, W. Zhong, G. Sui and X. Yang, *Polym. Chem.*, 2017, **8**, 2016–2027.

41 J. H. Hildebrand, *Regular and related solutions: the solubility of gases, liquids, and solids*, 1970.

42 H. Li, Y. Zhao and Y. Ning, *J. Hazard. Mater.*, 2019, **362**, 303–310.

43 T. Steiner and G. R. Desiraju, *Chem. Commun.*, 1998, 891–892.

44 J. Blackwell and K. H. Gardner, *Polymer*, 1979, **20**, 13–17.

45 C. Hepburn, *Prog. Polym. Sci.*, 1991, **16**, 695–836.

46 Y. Du, J. Zheng and G. Yu, *Polymers*, 2020, **12**, 403.

47 S. Kawana and R. Jones, *Phys. Rev. E: Stat., Nonlinear, Soft Matter Phys.*, 2001, **63**, 021501.